9-1-2017

Intracranial EEG fluctuates over months after implanting electrodes in human brain.

Hoameng Ung
University of Pennsylvania

Steven N. Baldassano
University of Pennsylvania

Hank Bink
University of Pennsylvania

Abba M. Krieger
University of Pennsylvania

Shawniqua Williams
University of Pennsylvania

See next page for additional authors

Authors
Hoameng Ung, Steven N. Baldassano, Hank Bink, Abba M. Krieger, Shawniqua Williams, Flavia Vitale, Chengyuan Wu, Dean Freestone, Ewan Nurse, Kent Leyde, Kathryn A. Davis, Mark Cook, and Brian Litt

HHS Public Access

Author manuscript

J Neural Eng. Author manuscript; available in PMC 2018 October 01.

Published in final edited form as:

J Neural Eng. 2017 October 01; 14(5): 056011–. doi:10.1088/1741-2552/aa7f40.

Intracranial EEG Fluctuates Over Months After Implanting Electrodes in Human Brain

Hoameng Ung[1,2,*], **Steven N. Baldassano**[1,2], **Hank Bink**[1,2], **Abba M Krieger**[3], **Shawniqua Williams**[2,4], **Flavia Vitale**[1,2], **Chengyuan Wu**[5], **Dean Freestone**[6], **Ewan Nurse**[6,7], **Kent Leyde**[8], **Kathryn A Davis**[2,4], **Mark Cook**[6], and **Brian Litt**[1,2,4]

[1]Department of Bioengineering, University of Pennsylvania, Philadelphia, PA, USA

[2]Center for Neuroengineering and Therapeutics, University of Pennsylvania, Philadelphia PA, USA

[3]Department of Statistics, University of Pennsylvania, Philadelphia, PA, USA

[4]Department of Neurology, Hospital of the University of Pennsylvania, Philadelphia, PA, USA

[5]Department of Neurosurgery, Thomas Jefferson University Hospitals, Philadelphia, PA, USA

[6]Department of Medicine, St. Vincent's Hospital, University of Melbourne, Victoria, Australia

[7]Department of Biomedical Engineering, University of Melbourne, Victoria, Australia

[8]Cascade Medical Devices, Seattle, Washington

Abstract

Objective—Implanting subdural and penetrating electrodes in the brain cause acute trauma and inflammation that affect intracranial electroencephalographic (iEEG) recordings. This behavior and its potential impact on clinical decision-making and algorithms for implanted devices have not been assessed in detail. In this study we aim to characterize the temporal and spatial variability in continuous, prolonged human iEEG recordings.

Approach—Intracranial electroencephalography from 15 patients with drug-refractory epilepsy, each implanted with 16 subdural electrodes and continuously monitored for an average of 18 months, was included in this study. Time and spectral domain features were computed each day for each channel for the duration of each patient's recording. Metrics to capture post-implantation feature changes and inflexion points were computed on group and individual levels. A linear mixed model was used to characterize transient group-level changes in feature values post-implantation and independent linear models were used to describe individual variability.

Main Results—A significant decline in features important to seizure detection and prediction algorithms (mean line length, energy, and half-wave), as well as mean power in the Berger and high gamma bands, was observed in many patients over 100 days following implantation. In addition, spatial variability across electrodes declines post-implantation following a similar timeframe. All selected features decreased by 14–50% in the initial 75 days of recording on the

[*]Corresponding Author Contact Information. Hoameng Ung, 301 Hayden Hall, 3320 Smith Walk, Philadelphia PA 19104, Office phone: 215-746-4850, hoameng@mail.med.upenn.edu.

group level, and at least one feature demonstrated this pattern in 13 of the 15 patients. Our findings demonstrate that iEEG signal features demonstrate increased variability following implantation, most notably in the weeks immediately post-implant.

Significance—These findings suggest that conclusions drawn from iEEG, both clinically and for research, should account for signal variability and that properly assessing the iEEG in patients, depending upon the application, may require extended monitoring.

Keywords

Brain Machine Interface; Long-term EEG; Electroencephalography; Epilepsy; Electrodes; Intracranial

INTRODUCTION

Intracranial electrodes are routinely used to map cortical networks when patients with drug-resistant, localization-related epilepsy are evaluated for epilepsy surgery[1]. Emerging technologies of closed-loop stimulation and brain-machine interface (BMI) technologies are broadening applications for chronic intracranial electrodes to include therapeutic electrical stimulation, seizure monitoring and warning systems, responsive neurostimulation, and adaptive deep brain stimulation[2–6]. Each application benefits from a thorough understanding of acute changes at the brain-electrode interface and how they affect recorded signals.

Electrode implantation causes acute trauma and an immunologic reaction that has been studied extensively[7–12]. Greater than 50% of patients have histopathological changes from electrode implantation as soon as one day after surgery[13]. This reaction has been associated with changes in electrode impedance[8,14–17] and overall signal quality[8,18,19]. However, no studies have characterized the effect of such changes on signal features other than signal-to-noise ratios and impedance measurements. Furthermore, no analysis has been performed on long-term continuous recordings in humans, which has direct implications for algorithm design and clinical interpretation. For example, the Responsive Neurostimulator (RNS®) System (NeuroPace; Mountain View, CA) currently requires physicians to manually tune algorithm parameters to maintain high-sensitivity seizure detection over extended use[3]. Likewise, in the NeuroVista (Seattle, WA) seizure advisory system study, feature drift was observed and algorithm retraining was necessary for months after implantation[2]. Characterizing changes in signal features (line length, area, energy, half-wave, power) used in these two devices for seizure detection would improve algorithm development, patient-specific customization, and clinical interpretation of recorded results[6,20–26].

Similarly, short-term intracranial EEG (iEEG) is the gold standard for guiding surgical treatment of localization-related epilepsy, yet less than 66% of cases result in long-term seizure remission[27]. In an attempt to electrographically localize the seizure onset zone, iEEG recordings are obtained in an inpatient hospital setting, typically over 1–2 weeks. If reactions occurring at the brain-electrode interface affect recorded signals to the degree that extracted biomarkers become unreliable, then clinical decisions based on these features should be questioned. In addition, emergence of biomarkers such as high-frequency

oscillations for surgical planning adds importance to assessing time-dependent changes in spectral characteristics[28].

In this study, we evaluate continuous subdural iEEG recordings from 15 ambulatory human patients recorded for an average of 18 months. We aim to characterize temporal and spatial variability across electrodes, focusing on time and spectral domain features that are of clinical and algorithmic interest. By incorporating features used in the NeuroPace RNS® device as well as the original NeuroVista trial, our findings will have immediate impact on algorithms currently utilized in patient management in addition to informing future algorithm development.

METHODS

Dataset

Fifteen patients with drug resistant, localization-related epilepsy were each implanted with 16 subdural electrodes during a trial of the NeuroVista seizure prediction device[2]. Electrodes were placed unilaterally over the region containing the presumed seizure onset zone as determined by standard clinical evaluation. In patients with bilateral temporal lobe seizures, leads were placed over the hemisphere observed to generate the greater number of seizures. Patient demographics and recording duration are given in Table 1. Further details about the human patients are discussed in the original manuscript reporting this trial[2].

Recording device

The NeuroVista electrode array consists of four electrode strips each with four medical grade platinum-iridium (90/10) contacts. Electrodes, each with a 2 mm exposed contact diameter, were spaced either 10mm or 20mm apart for optimal coverage of the seizure onset zone and surrounding areas (Figure S1). The electrodes were connected to a hermetically sealed subclavicular implantable telemetry unit that sampled each of the 16 channels at 400 Hz. The telemetry unit amplified, digitized, and buffered the data, which was then wirelessly transmitted to an external belt-worn computing and warning device. Limited telemetry range and patient-related factors (e.g. misplaced external device, failure to maintain battery charge levels) occasionally interrupted data acquisition throughout the trial, resulting in data gaps. Subsequent to the study, the data were converted to the Multiscale Electrophysiology Format (MEF)[29], ported to ieeg.org, and accessed in MATLAB using the IEEG-Portal[30] toolbox for data analysis.

Feature Extraction

Each channel was initially low-pass filtered at 190 Hz with a third order Butterworth filter. Four time-domain features (line length[21], area[25], energy, and half-wave amplitude[31]) as well as average spectral power in delta [0.1–4 hz], theta [4–8], alpha [8–12], beta [12–30], gamma [30–100], and high-gamma [100–180] bands were computed. Additional sub-band trends were also calculated for gamma and high gamma to account for both line noise and an expected decrease in power with increasing frequency.

These features were selected to represent those commonly used in algorithms to detect epileptiform activity as well as common, interpretable spectral bands. Line length, for example, has been shown to be an efficient feature for detecting seizures by capturing transient increases in frequency and voltage that occur during a seizure[21]. The time domain features included in this study are also easily implemented in devices with limited computational resources. Line length, area, and half-wave are used in the FDA-approved NeuroPace RNS® for ambulatory seizure detection and line length, area, and energy were used in the original NeuroVista trial for seizure prediction[2]. Therefore, tracking these time-domain features has immediate implications for human implantable devices. The selected spectral bands are observed in normal and abnormal human physiological processes and are commonly used in the interpretation of EEG. For example, delta power is increased during specific stages of sleep and in some patients with brain lesions. Similarly, alpha power indicates a relaxed state but may be pathologically elevated in comatose patients.

Specifically, *line length* is the absolute derivative of signal amplitude[21]. *Area* is defined as the absolute voltage amplitude[23,24]. The *energy* of a signal is calculated as the squared voltage amplitude. The *half wave* feature represents the amplitude and duration of a signal after segmentation based on local minima and maxima[25,26]. From the segmentation, the amplitude and duration can be extracted and reflects energy at various frequencies depending on tunable parameters. Here, the average half-wave amplitude is used. Spectral power was calculated using Welch's power spectral density estimate. Additional details of feature calculations are provided in the supplementary materials.

The mean value of each feature was calculated in 5-minute moving windows with no overlap over each channel for each patient. These values were subsequently averaged across 24-hour segments within each channel to reduce data dimensionality and account for changes due to circadian rhythm.

Preprocessing

Artifacts, which were rare, were identified for the majority of patients through visualization of extracted features. Outliers were manually identified based on large spikes or large drops in each feature space and, if verified to arise from artifacts on raw EEG, were removed from corresponding channels across all features. Large increases in feature values were often correlated with short periods of line noise harmonics or transient epileptiform activity (seizures), particularly if these periods occurred in windows overlapping with data gaps as they would not be averaged out. Large decreases correlated most often with multiple electrode drop offs. In total, 396 out of 6565 days, or 6.1% of available days, were removed. Examples of removed artifacts are shown in the supplementary materials (Figure S2).

Statistical Analysis

Statistical analyses were performed in R. For each patient and for each day, the mean and coefficient of variation (standard deviation/mean) across channels were calculated for each feature. The coefficient of variation captured spatial variability normalized by the mean feature value. Before averaging across patients for group level analysis, feature values for each channel and coefficients of variation for each patient were independently normalized to

[0–1] based on 95% of the values. Individuals were also analyzed independently to understand variability among patients.

Group statistics

Group-level feature values were initially observed to decrease post-implantation before stabilizing. Based on this observation, a reference distribution, intended to represent a period after a post-implantation effect, was obtained from the mean and standard deviation of values from day 200 to day 500. Though there is variability in feature values during this period, the purpose of this approach is to model the range of feature values as a comparator for the immediate post-implantation phase without making a prior assumption of stabilization. As patients dropped out due to variable recording durations, these times were selected to include at minimum the majority of patients (8/15). Means corresponding to a critical value of a one-sided z-test with significance of p=0.05 (z=1.645) were selected as the reference threshold. Values greater than this threshold were significantly different than the distribution of values expected for a particular feature. The number of days required to enter this predefined reference range is reported. Furthermore, as features were observed to continue to decrease after entering the reference range, an inflexion point was calculated as the day when the derivative of feature values crosses 0.

To model the group level change in feature values in the initial 75 days post-implantation, a linear mixed model (equation 1) was used with day as a covariate and feature value (averaged over channels) as a response variable. Linear mixed models allow modeling of patient-specific trends and are also robust to missing data. Separate models were fit for each feature and estimates for group level fixed effects (β_1), intercepts (β_0), and random effects (b_{0i}, b_{1i}) were obtained. As the feature value on day 1 and the rate of change across days 1–75 may vary with each patient, a random intercept (b_{oi}) and slope (b_{1i}) was used. This accounts for longitudinal measurements and assumes that each patient is drawn from a population. The Wald t-statistic was used to determine the significance of any trend across time.

$$Y_{\mathrm{ij}}=\beta_0+\beta_1 t_{\mathrm{ij}}+b_{0i}+b_{1i}t_{\mathrm{ij}}+\varepsilon_{\mathrm{ij}} \quad (1)$$

where $b_{0i} \sim N(0, \tau^2)$, $b_{1i} \sim N(0, \tau_{1i}^2)$, Y_{ij} denotes the j'th feature value for patient i, t_{ij} indexes the day after implantation, b_{0i} and b_{1i} are random intercepts and slopes for each patient, for patient *i*.

Individual statistics

Changes in feature values were observed to follow a linear trend post-implantation, though there was variability present among patients. To determine the average rate of change in feature values, independent linear models (equation 2) were fit on the first 75 days post-implantation for each feature, for each patient with time in days as the covariate. This 75-day period was selected to model the initial rate of change in feature values observed across many patients. The significant main effects of time are reported after adjusting for false discovery rate (FDR) of 0.05 (Benjamini-Hochberg[32]). These main effects (β_1) represent the

rate of decay (or growth) of a feature over time (t) and whether this rate is statistically different than 0 (indicating stability).

$$Y=\beta_0+\beta_1 t+\varepsilon \quad (2)$$

where Y denotes the feature value for a given patient, t denotes the day after implantation, β_0, β_1 are the intercepts and slopes. This model was fit individually for each patient and each feature.

Days to reference range and inflexion points were also calculated for individual patients. Specifically, in order to determine an accurate reference distribution, only patients with more than 50 days within our 200–500 day range were included. Furthermore, a few patients were observed to remain unstable throughout the recording period. To identify these patients, a linear model, similar to equation 2, was fit to the feature values within this reference distribution and patients with a significant linear trend that explains more than 50% of the variance (adjusted R^2 > 0.5) were excluded from the calculations. This ensured that the reference range, when calculated individually, captured an appropriate reference distribution.

Code Availability

Code is available at http://www.github.com/hoameng/transients-2017.

RESULTS

Temporal variability

The day that each feature enters our predefined reference distribution and the inflexion day are given in Table 2 with corresponding feature values in Table 3. Time domain features show a prominent transient response in the first 100 days after implantation (Figure 1). Specifically, line length, half-wave amplitude, and energy are highest at implantation, enter the reference range between days 27 and 48, and decrease between 36% and 42% in the first 75 days (Table 4). Area follows the same initial decreasing trend, but due to fluctuations throughout the recording period, feature values remain within our defined reference distribution. In addition to these features, we tested root mean square (RMS) and the first and second derivative of the voltage. The corresponding figures are given in Figure S5 and S6.

All spectral bands show a transient decline in power from day 1 that falls below the calculated threshold by day 100 (Figure 2). The average power decline from day 1 to day 75 was 40% (Table 4).

Spatial variability

The coefficient of variation for line length and half-wave declined in the first 100 days, whereas the coefficients of variation for area and energy fluctuated within the reference range (Figure 3). The coefficient of variation for spectral power in the delta, theta, alpha, and beta bands also declined in the initial stages of recording. Increasing frequency bands were inversely related to the magnitude of the post-implantation effect (Figure 4). These findings

indicate that spatial variability of lower frequency power bands across channels decreases over time, entering our defined reference distribution between 37–52 days after implantation.

The normalized feature values for all features at day 1, number of days to cross the reference threshold, and number of days to inflexion point are given in Table 3 for both temporal and spatial trends.

Individual Fits

Beta estimates for each patient and each feature are shown in Figure 5, with corresponding p values in Figure S7. Of the 135 patient-feature combinations, 83 displayed a statistically significant linear trend after FDR correction, 79 of which declined in the initial 75 days. Fourteen of the 15 patients had significantly decreasing values in at least one feature. Patient 3 and 5's recordings were more stable in the spectral domain, resulting in insignificant beta estimates across all power bands. Calculated line length, beta power, and gamma power for all subjects are shown in Figures 6 and 7. There was also patient variability in the days to reference threshold and inflexion points as seen in Figures 6–7 and Table S1 and S2.

DISCUSSION

In this study we analyzed continuous long-term ambulatory recordings from subdural iEEG electrodes implanted in humans and characterize the temporal and spatial variability of time and spectral domain features frequently used in research and device algorithms. This study is unique as it explores the only known dataset of long-term continuously recorded human iEEG spanning an average of 1.5 years, as opposed to episodic, brief recordings lasting up to a few weeks. Our findings may directly impact the clinical management of human patients, since the selected features represent those used in current implantable devices (discussed further below). We show on a group level that in the majority of features there is an initial decline in the mean values that reaches an inflexion point roughly 100 days after implantation (Figures 1, 2, Table 2). This trend in feature values is consistent on the group level (14/15 patients), although there is significant variability among patients beyond the initial weeks (Figures 5–7). Furthermore, spatial variability between channels for line length, half-wave, and a number of spectral bands (delta to beta) decreases post-implantation before stabilizing in a similar time frame. These observations demonstrate an initial period of decline in iEEG recordings features relative to long-term trends. While these patterns are present on the group level, there is significant inter-patient variability that is worth noting, suggesting a need to further study individual characteristics to adequately predict and control for transient patient-specific changes in EEG signals

Temporal variability

On a group level, we found a significant initial decline in the majority of feature values, reaching a point of inflexion near day 100 (Figure 1, Table 2). Several of these features, such as line length, energy, and power, have an expected correlation that is reflected in similar temporal trends (Figure 1, 2). Furthermore, the strong correlation between line length and

power (Table S3), coupled with the dissimilarity in trends with area, suggests that line length in practice is more sensitive in recording changes in frequency than voltage amplitude.

To ensure our findings were not significantly influenced by main line noise frequency and to help account for decreases in power with increasing frequency, we conducted an additional analysis for gamma and high gamma sub-bands. Gamma sub-bands (30–45 Hz and 55–100 Hz) displayed similar temporal trends to the full 30–100 Hz band despite removing line noise at 50 Hz, stabilizing on similar days (~30–40 days) (Figure S3). High gamma sub-bands (100–140 Hz and 140–180 Hz) also displayed similar trends (Figure S4). These figures suggest that our findings are consistent regardless of line noise or higher frequencies.

These findings demonstrate the temporal variability present in time and frequency domain features following implantation. Line length and half-wave, two features used in the NeuroPace[25] and NeuroVista[2] algorithms, decrease by over 30% in the first 75 days as estimated by a linear fit (Table 4). Using these features for seizure detection or prediction may lead to decreased sensitivity over time as feature values trend down. The lack of stable feature baselines may also present challenges in using early data for device training. Furthermore, power features decrease dramatically by over 40% on average over time (Table 4). This drift must be accounted for in chronic neurodevices, either by directly modeling the change or waiting until stabilization before optimizing algorithms. Finally, changes in RNS® detections observed in the first few months after a chronic implant should be interpreted with caution, so as not to falsely attribute perceived clinical response to early changes in therapeutic stimulation parameters.

Spatial variability

It is also important to capture the variability between electrodes to inform algorithms that utilize spatial features (measurements between channels). If the processes causing post-implantation changes affect all electrodes equally, the mean may decrease while the coefficient of variation, which is normalized by the mean, would remain constant. However, we observed that the spatial variation of line length, half-wave, and spectral power decreases over time (Figures 3, 4) and, similar to temporal variability, this effect is more significant in the lower frequencies. Notably, while the spatial variation enters the defined reference distribution later than the temporal variation, suggesting a different rate of decline, the coefficients of variation form reaches our calculated inflexion point roughly the same time (day 100) as their corresponding mean feature values (Table 2). A decrease in the coefficient of variation indicates that the standard deviation relative to the mean is decreasing. This may suggest that the processes responsible for the trend in mean feature values affect each electrode differently, and the magnitude of this difference decreases over time. As a result, we can expect any spatial measures of iEEG to be unstable in the initial periods after an implant. This may be accounted for by variability in electrode locations. For instance, sub-temporal electrodes may experience greater movement due to the anatomical location, which results in a greater tissue reaction (discussed further below) at the brain-electrode interface relative to more stable electrodes. This may affect voltage recordings differently for these electrodes relative to the mean effect across all electrodes, causing the observed decrease in the coefficient of variation when averaged over a day.

Previous studies

Histological changes at the brain-electrode interface likely explain the observed feature variability following implantation, since both follow a similar time course. These interactions have been studied extensively in electrodes implanted into animals and humans[7,9,10,18] and involve an acute inflammatory response followed by chronic fibrosis that significantly diminishes by 6–8 weeks[10,33–35]. Notably, many of these past studies analyzed the impact of intracortical electrodes, which penetrate the cortical surface and have an increased burden on the brain. Several studies in non-human primates and rats with subdural electrodes have shown minimal damage to the cortex but fibrous tissue encapsulation over time[36–38] that subsequently lead to greater changes in electrode impedance relative to intracortical electrodes[14,39,40]. Since electrode impedance directly impacts our calculated features, we relate our observations to previously reported changes in impedance in studies of subdural iEEG. Specifically, subdural electrodes implanted in rats have shown an increase in impedance in the first 30 days after implantation[38] that stabilizes after week 18[37,38]. On histology, fibrous tissue encapsulation was observed surrounding the electrodes. Interestingly, a recent study in non-human primates recorded for over 600 days reported root-mean-square (RMS) voltage stability at 300 days, which is much later than the stability we observe in signal features[36] and possibly suggests different timescales between non-human primates and humans. In fact, we separately calculated RMS as well and time to stabilization/inflexion was 17/108 days, respectively (Figure S5). This difference might be related to differences in immune response in these animals, sterile conditions of the implants or perhaps mechanical or material factors. In humans, Sillay et al. recently showed that impedance in the NeuroPace RNS® subdural electrodes increases an estimated 30% from day 1 to day 84 after implantation and stabilizes by four months[39]. This is similar to the magnitude of change that we observed in our time and spectral features from day 0 to day 75 (Table 4), suggesting that our observed changes are related to previously described changes in impedance. However, it should be noted that the RNS® impedance recordings were collected intermittently with limited temporal resolution, whereas our recordings were continuous. Notably, while we observe high degree of similarity between the time courses of each of the power bands, the decrease in power was greatest in lower frequencies. These changes could be motivated by an increase in both the resistive and capacitive impedance due to tissue encapsulation, as previously reported in microelectrodes[41].

Individual variability

While group level trends show a clear initial trend in feature values, there is also substantial individual variability that is important to consider. At least two or more features for 13 patients displayed a significant trend in the initial 75 days (Figure 5) before entering into a relatively stable state. This suggests that many patients on an individual level also experience an initial decline in feature values. Interestingly, beyond this initial period, the feature trends display more variability and the patients appear to group into several cohorts. For example, line length trends shows patients that appear stable (3), quickly enter a reference range (1, 5, 7, 10, 14, 15), show a more gradual trend towards a defined reference range (4, 6, 8, 9, 11, 13), or appear to be relatively unstable (2, 12) (Figure 6). These patterns are similar for beta power (Figure 7). In two patients (3 and 5), all but one feature was stable (Figure 5, Figure S6). Patients 3 and 5 with stable EEG were the two youngest individuals, perhaps suggesting

that these patients may have a more robust wound healing response than other patients[42], though we do not have enough data to draw any definitive conclusions. Alternatively, it is possible that surgical complications and electrode location may impact these values. Furthermore, patients with a significant decline in one feature tend to have a similar trend in other features, suggesting a common source likely due to changes at the brain-electrode interface. The observed patient level variability suggests a need for patient-specific control during iEEG recording, and additional insights may be found as chronic invasive recording becomes more widely available.

Although 95% of all statistically significant features initially decreased over time, four features displayed increasing values. Though it is difficult to explain these differences, it is clear the majority of patients demonstrate significant initial trends over time (Figure 5).

Clinical Implications

Our study is the first of its kind to extend observations of RMS and impedance to signal features in continuous recordings, a next step towards translating these findings into clinical care. Variability in signal properties has ramifications for emerging closed loop systems for the treatment of drug-resistant epilepsy[3], development of brain-machine interfaces and clinical trial design. These systems must be cognizant of post-implant variability, suggesting a need for strategies to either algorithmically control for this instability or otherwise optimize on an individual basis.

As an example, current common practice using the NeuroPace implantable responsive neurostimulator includes a postoperative observation period to capture patient seizures for algorithm training. The duration of this period varies from center to center, and parameters for seizure detection and closed-loop stimulation are typically adjusted at each subsequent clinic visit based on the number and types of detections and on the clinically evident seizures reported since the last visit. The detection parameters, which are based on area, line length, and half-wave, are then tuned based on a feature threshold. Once a seizure is detected, the device responsively stimulates in an attempt to abort the seizure. The observed changes suggest a need for frequent tuning of feature parameters for seizure detection on a patient-by-patient basis in order to ensure accurate detection of electrographic seizures. Clinicians should also set expectations for their patients that the timeframe for optimization of detection and stimulation parameters necessarily includes a potentially prolonged period for stabilization.

It is also important to determine the impact of these changes on clinical biomarkers that are used in the care of the drug resistant epilepsy population. Acute implantation can induce interictal epileptiform activity and seizures that do not accurately represent a patient's underlying disorder[43,44]. This may be a result of direct effects, such as of trauma, electrode contact with the cortical tissue, or complications of electrode placement such as hemorrhage, fluid collections or cerebral edema[44]. Seizure onset localization relies on identifying subtle electrographic changes that are spatially distinct, so any changes in spatial variability may interfere with the localization procedure. Of interest, there is evidence that patients who appear to have multifocal onset seizures immediately after electrode implantation during standard clinical evaluation localize to one predominant area in the chronic steady state,

eventually resulting in seizure-free outcome after surgery[45]. This provides at least circumstantial evidence that the chronic steady state may better reflect a patient's baseline than alterations of the network from implantation. In this dataset, clinical seizure semiology typically did not change in the chronic state from pre-implantation in most of our patients, giving some reassurance that these effects are limited in scope. However, it has been demonstrated in that seizures can have similar clinical appearance while arising from different parts of an epileptic networks, sometimes with different EEG signatures. A recent study by our group shows this phenomenon in a long-term canine model[46]. Classifying seizures and mapping their temporal trends is an ongoing project in our laboratory.

Limitations

In this analysis, we defined a "reference" distribution to occur between day 200 and day 500. Although this is an arbitrary definition, we believe that this captures the variability in feature values after any initial post-implantation changes, regardless of how the features behave afterward. By modeling this distribution, increased variability during this period will increase the reference threshold and raise the feature values necessary to demonstrate a change in trends post-implantation relative to longer term recordings. Despite this variability, which is difficult to explain on our time scale, the feature value trends post-implantation are important to describe both on an individual and group level.

An interesting question to consider from our findings is whether the steady state observed after stabilization of chronic intracranial recordings represents "ground truth". It is possible that recordings immediately post-implantation more accurately reflect neural activity, and that chronic recordings are confounded due to changes at the brain-electrode interface. This question is particularly important when considering epilepsy biomarkers, such as interictal epileptiform discharges and seizures, and interpreting what their temporal and spatial distributions mean with respect to the fundamental mechanisms underlying epileptic networks. Like the Heisenberg Uncertainty Principle, unfortunately, it is clear that our measurements of the iEEG, for which there is not currently a noninvasive alternative, perturb the system and may induce chronic change. At present, iEEG studies provide the best way of assessing an epileptic network's broad band activity on a clinical scale, even taking this limitation into consideration. It will be important in future studies from this unique data archive to determine if localization of seizures and interictal epileptiform discharges change similarly over the first 100 days, which may have more important consequences for current epilepsy surgery and ablative therapies. Should spatial localizations change, as the paper by DiLorenzo et al suggests, either due to brain disruption or merely inadequate temporal sampling, this may require a paradigm shift in the duration of monitoring required to localize epileptic networks for intervention. This might require that we monitor patients in the ambulatory setting for months, rather than weeks in the hospital.

CONCLUSION

We have shown that calculated features of human subdural recordings decline after implantation and exhibit a temporal and spatial post-implantation response that requires roughly 100 days to enter a reference range. This response was present in the majority of our

patients, though there was significant variability between individual recordings. Our findings directly explain observed trends in human neurodevice implants and show that systems that use or interpret subdural electrode recordings must account for signal variability on a patient level for optimal performance. In addition, further study is warranted to better explain inter-subject differences.

Supplementary Material

Refer to Web version on PubMed Central for supplementary material.

Acknowledgments

Funding

This study was funded by National Institutes of Health (NIH) and the Mirowski Family Foundation grants through the University of Pennsylvania: NIH U01NS073557, T32 NS091006, NIH R01NS099348. The International Epilepsy Electrophysiology Portal is funded by the NIH (U24NS063930).

References

1. Noachtar S, Rémi J. The role of EEG in epilepsy: A critical review. Epilepsy and Behavior. 2009:22–33. [PubMed: 19248841]
2. Cook MJ, O'Brien TJ, Berkovic SF, et al. Prediction of seizure likelihood with a long-term, implanted seizure advisory system in patients with drug-resistant epilepsy: A first-in-man study. Lancet Neurol. 2013; 12:563–71. [PubMed: 23642342]
3. Morrell MJ. Responsive cortical stimulation for the treatment of medically intractable partial epilepsy. Neurology. 2011; 77:1295–304. [PubMed: 21917777]
4. Little S, Pogosyan A, Neal S, et al. Adaptive deep brain stimulation in advanced Parkinson disease. Annals of Neurology. 2013
5. Nicolas-Alonso LF, Gomez-Gil J. Brain computer interfaces, a review. Sensors. 2012:1211–79. [PubMed: 22438708]
6. Wu C, Sharan AD. Neurostimulation for the treatment of epilepsy: A review of current surgical interventions. Neuromodulation. 2013:10–24. [PubMed: 22947069]
7. Polikov VS, Tresco PA, Reichert WM. Response of brain tissue to chronically implanted neural electrodes. J Neurosci Methods. 2005; 148:1–18. [PubMed: 16198003]
8. Prasad A, Sanchez JC. Quantifying long-term microelectrode array functionality using chronic in vivo impedance testing. J Neural Eng. 2012; 9:26028.
9. Van Kuyck K, Welkenhuysen M, Arckens L, et al. Histological alterations induced by electrode implantation and electrical stimulation in the human brain: a review. Neuromodulation. 2007; 10:244–61. [PubMed: 22150838]
10. Sun, Da, Yu, H., Spooner, J., et al. Postmortem analysis following 71 months of deep brain stimulation of the subthalamic nucleus for Parkinson disease. J Neurosurg. 2008; 109:325–9. [PubMed: 18671648]
11. Yuen GH, Bullara FA. Tissue response to potential materials implanted neuroprosthetic subdurally. 1986
12. Hanisch U-K. Microglia as a source and target of cytokines. Glia. 2002; 40:140–55. [PubMed: 12379902]
13. Fong, JS., Alexopoulos, AV., Bingaman, WE., et al. Am J Clin Pathol. Vol. 138. The Oxford University Press; 2012. Pathologic findings associated with invasive EEG monitoring for medically intractable epilepsy; p. 506-10.
14. Wu C, Evans JJ, Skidmore C, et al. Impedance variations over time for a closed-loop neurostimulation device: Early experience with chronically implanted electrodes. Neuromodulation Nov. 2013:46–50.

15. Lind G, Gällentoft L, Danielsen N, et al. Multiple implants do not aggravate the tissue reaction in rat brain. PLoS One. 2012; 7:e47509. [PubMed: 23091629]
16. Biran R, Martin DC, Tresco PA. Neuronal cell loss accompanies the brain tissue response to chronically implanted silicon microelectrode arrays. Exp Neurol. 2005; 195:115–26. [PubMed: 16045910]
17. Cogan SF. Neural stimulation and recording electrodes. Annu Rev Biomed Eng. 2008; 10:275–309. [PubMed: 18429704]
18. Liu X, McCreery DB, Carter RR, et al. Stability of the interface between neural tissue and chronically implanted intracortical microelectrodes. IEEE Trans Rehabil Eng. 1999; 7:315–26. [PubMed: 10498377]
19. Ludwig KA, Uram JD, Yang J, et al. Chronic neural recordings using silicon microelectrode arrays electrochemically deposited with a poly(3,4-ethylenedioxythiophene) (PEDOT) film. J Neural Eng. 2006; 3:59–70. [PubMed: 16510943]
20. Davis R, Emmonds SE. Cerebellar stimulation for seizure control: 17-year study. Stereotactic and Functional Neurosurgery. 1992:200–8. [PubMed: 1439341]
21. Esteller R, Echauz J, Tcheng T, et al. Line length: an efficient feature for seizure onset detection. 2001 Conf Proc 23rd Annu Int Conf IEEE Eng Med Biol Soc. 2001; 2:1707–10.
22. D'Alessandro M, Esteller R, Vachtsevanos G, et al. Epileptic seizure prediction using hybrid feature selection over multiple intracranial EEG electrode contacts: a report of four patients. IEEE Trans Biomed Eng. 2003; 50:603–15. [PubMed: 12769436]
23. Echauz, J., Padovani, Da, Esteller, R., et al. Proceedings of the First Joint BMESEMBS Conference 1999 IEEE Engineering in Medicine and Biology 21st Annual Conference and the 1999 Annual Fall Meeting of the Biomedical Engineering Society Cat N. IEEE; 1999. Median-based filtering methods for EEG seizure detection; p. 439
24. Litt B, Esteller R, Echauz J, et al. Epileptic Seizures May Begin Clinical Study Hours in Advance of Clinical Onset:A Report of Five Patients. Neuron. 2001; 30:1–14. [PubMed: 11343635]
25. Sun FT, Morrell MJ, Wharen RE. Responsive Cortical Stimulation for the Treatment of Epilepsy. Neurotherapeutics. 2008; 5:68–74. [PubMed: 18164485]
26. Gotman J. Automatic seizure detection: improvements and evaluation. Electroencephalogr Clin Neurophysiol. 1990; 76:317–24. [PubMed: 1699724]
27. Téllez-Zenteno JF, Dhar R, Wiebe S. Long-term seizure outcomes following epilepsy surgery: a systematic review and meta-analysis. Brain. 2005; 128:1188–98. [PubMed: 15758038]
28. Haegelen C, Perucca P, Châtillon CE, et al. High-frequency oscillations, extent of surgical resection, and surgical outcome in drug-resistant focal epilepsy. Epilepsia. 2013; 54:848–57. [PubMed: 23294353]
29. Brinkmann, BH., Bower, MR., Stengel, KA., et al. Proceedings of the 31st Annual International Conference of the IEEE Engineering in Medicine and Biology Society: Engineering the Future of Biomedicine. EMBC; 2009. Multiscale electrophysiology format: An open-source electrophysiology format using data compression, encryption, and cyclic redundancy check; p. 7083-6.2009
30. Wagenaar, JB., Brinkmann, BH., Ives, Z., et al. International IEEE/EMBS Conference on Neural Engineering. NER; 2013. A multimodal platform for cloud-based collaborative research; p. 1386-9.
31. Gotman J, Gloor P. Automatic recognition and quantification of interictal epileptic activity in the human scalp EEG. Electroencephalogr Clin Neurophysiol. 1976; 41:513–29. [PubMed: 61855]
32. Yoav Benjamini YH. Controlling the False Discovery Rate: A Practical and Powerful Approach to Multiple Testing. J R Stat Soc Ser B. 1995; 57:289–300.
33. Schmidt S, Horch K, Normann R. Biocompatibility of silicon-based electrode arrays implanted in feline cortical tissue. Journal of Biomedical Materials Research. 1993:1393–9. [PubMed: 8263001]
34. Winslow, BD., Christensen, MB., Yang, WK., et al. Biomaterials. Vol. 31. Elsevier Ltd; 2010. A comparison of the tissue response to chronically implanted Parylene-C-coated and uncoated planar silicon microelectrode arrays in rat cortex; p. 9163-72.

35. Stice P, Gilletti A, Panitch A, et al. Thin microelectrodes reduce GFAP expression in the implant site in rodent somatosensory cortex. J Neural Eng. 2007; 4:42–53. [PubMed: 17409479]

36. Degenhart, AD., Eles, J., Dum, R., et al. J Neural Eng. Vol. 13. IOP Publishing; 2016. Histological evaluation of a chronically-implanted electrocorticographic electrode grid in a non-human primate; p. 46019

37. Henle C, Raab M, Cordeiro JG, et al. First long term in vivo study on subdurally implanted Micro-ECoG electrodes, manufactured with a novel laser technology. Biomed Microdevices. 2011; 13:59–68. [PubMed: 20838900]

38. Schendel, Aa, Nonte, MW., Vokoun, C., et al. The effect of micro-ECoG substrate footprint on the meningeal tissue response. J Neural Eng. 2014; 11:46011.

39. Sillay KA, Rutecki P, Cicora K, et al. Long-term measurement of impedance in chronically implanted depth and subdural electrodes during responsive neurostimulation in humans. Brain Stimul. 2013; 6:718–26. [PubMed: 23538208]

40. Kim YT, Hitchcock RW, Bridge MJ, et al. Chronic response of adult rat brain tissue to implants anchored to the skull. Biomaterials. 2004; 25:2229–37. [PubMed: 14741588]

41. Sankar V, Patrick E, Dieme R, et al. Electrode impedance analysis of chronic tungsten microwire neural implants: understanding abiotic vs. biotic contributions. Front Neuroeng. 2014; 7:13. [PubMed: 24847248]

42. Gosain A, DiPietro LA. Aging and Wound Healing. World Journal of Surgery. 2004:321–6. [PubMed: 14961191]

43. Fountas KN, King DW, Jenkins PD, et al. Nonhabitual seizures in patients with implanted subdural electrodes. Stereotact Funct Neurosurg. 2004; 82:165–8. [PubMed: 15528955]

44. Arya R, Mangano FT, Horn PS, et al. Adverse events related to extraoperative invasive EEG monitoring with subdural grid electrodes: A systematic review and meta-analysis. Epilepsia. 2013; 54:828–39. [PubMed: 23294329]

45. DiLorenzo DJ, Mangubat EZ, Rossi Ma, et al. Chronic unlimited recording electrocorticography-guided resective epilepsy surgery: technology-enabled enhanced fidelity in seizure focus localization with improved surgical efficacy. J Neurosurg. 2014; 120:1402–14. [PubMed: 24655096]

46. Ung H, Davis KA, Wulsin D, et al. Temporal behavior of seizures and interictal bursts in prolonged intracranial recordings from epileptic canines. Epilepsia. 2016

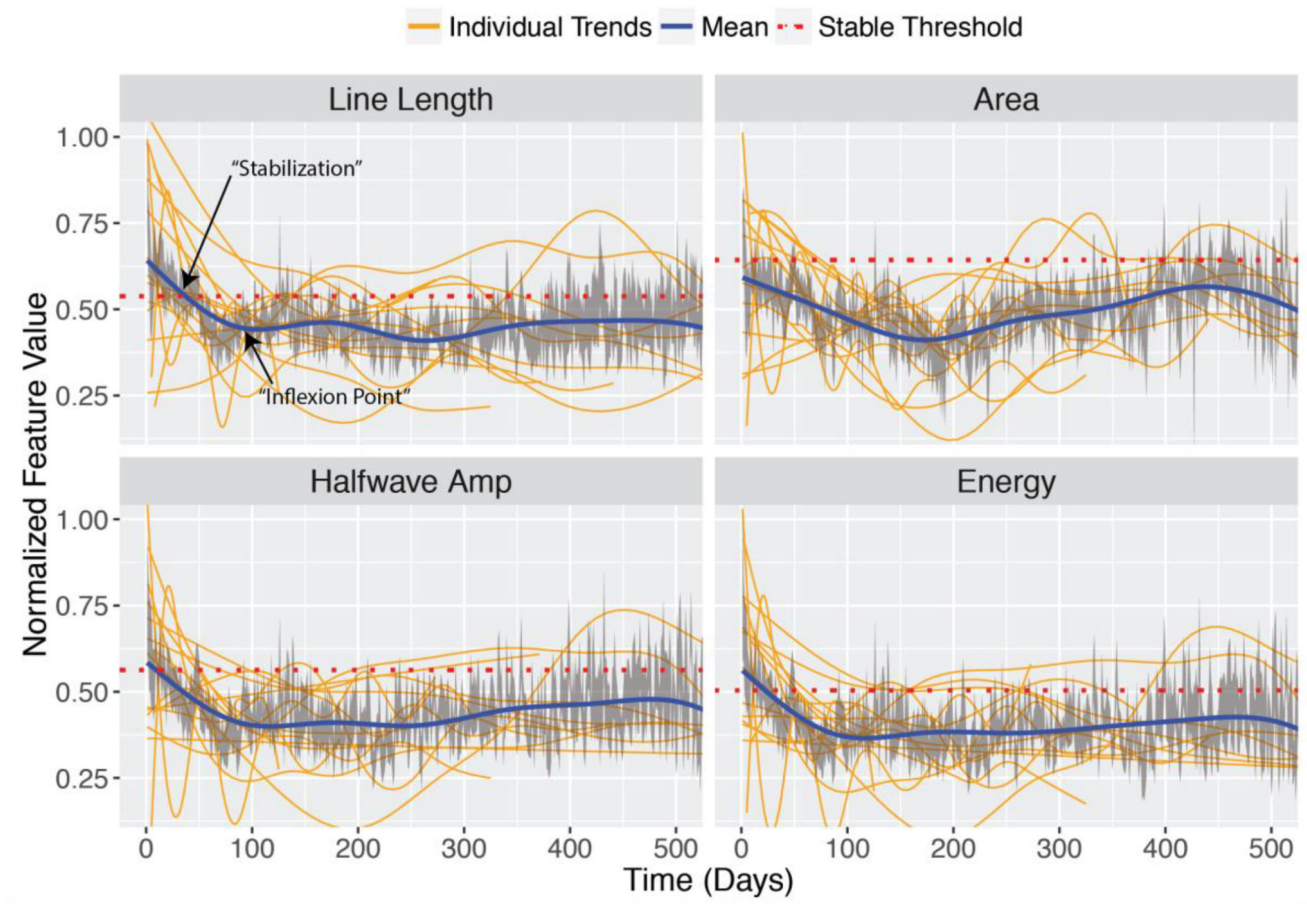

Figure 1. Temporal trend of time domain features

Mean line length, area, half-wave, and energy are shown with standard error (grey). Smoothed individual subject trends are shown in orange. Overlaid is the smoothed mean (blue) and reference threshold (red dashed line).

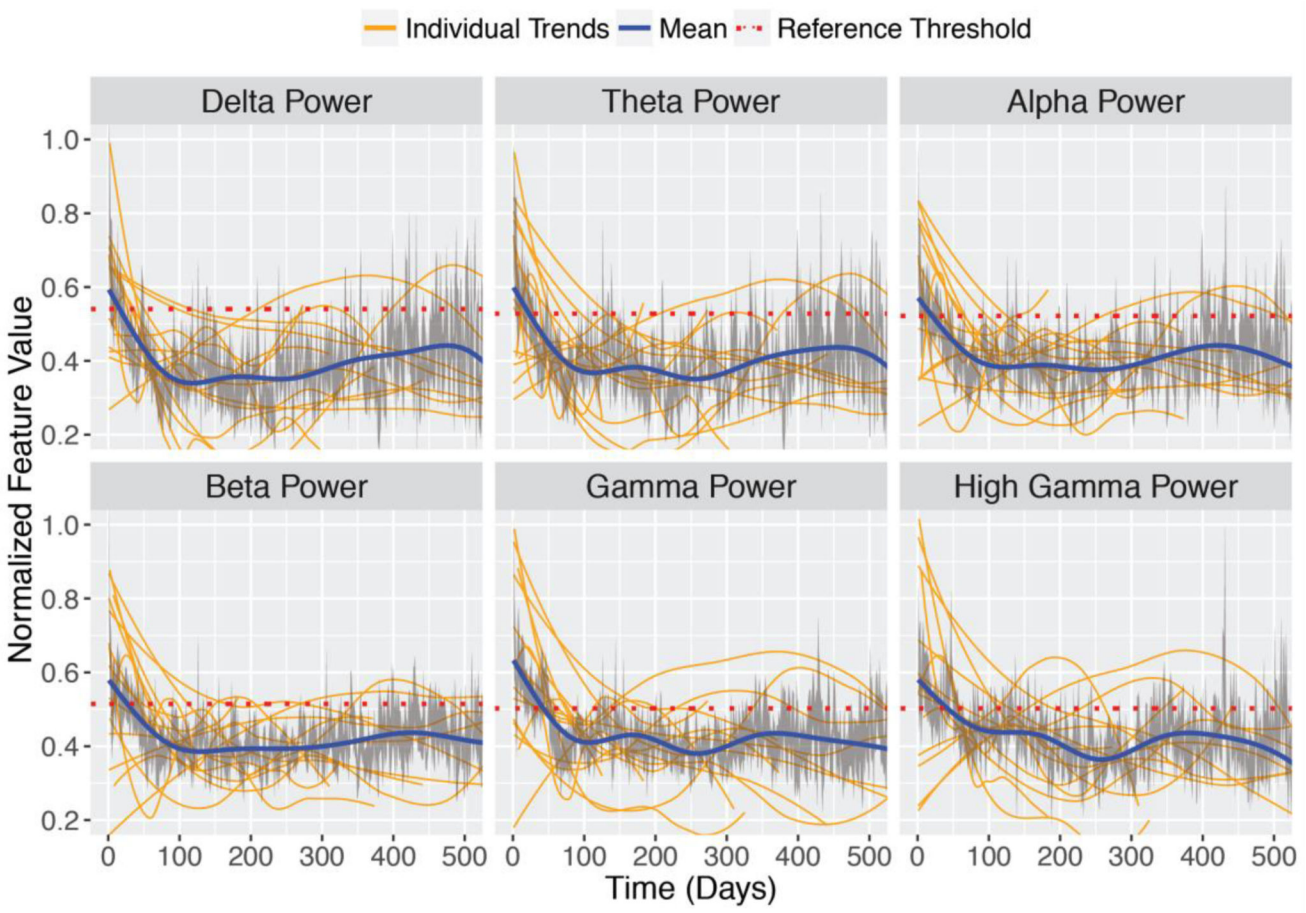

Figure 2. Temporal trend of spectral domain features

Average power in delta (0–4 Hz), theta (4–8), alpha (8–12), beta (12–30), gamma (30–100), and high-gamma (100–180) frequencies are shown, with standard error bars in grey. Smoothed individual subject trends are shown in orange. Overlaid is the smoothed mean (blue) and reference threshold (red dashed line).

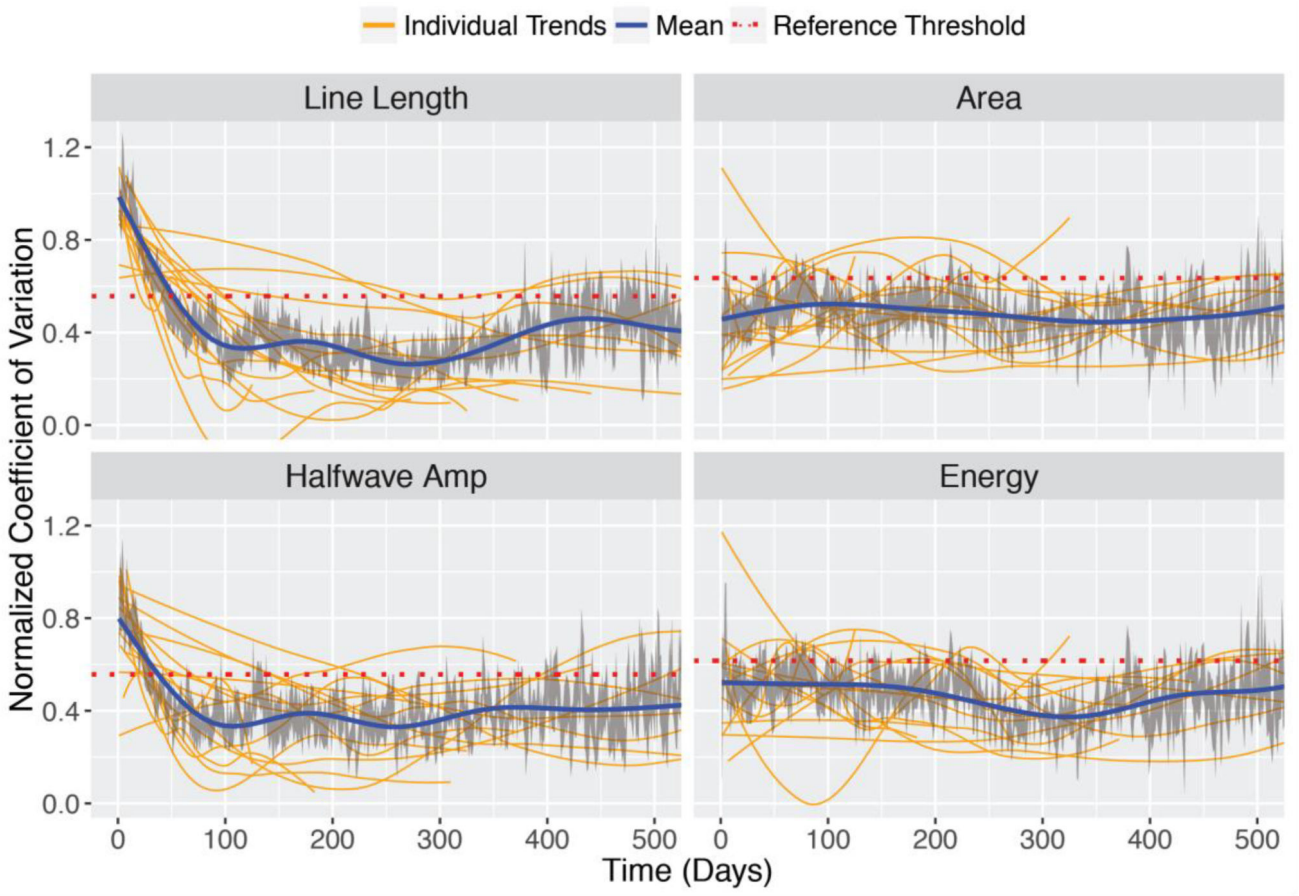

Figure 3. Coefficient of variation for time domain features

The mean and standard error of the coefficient of variation is shown for each time domain. Overlaid is the smoothed mean (blue) and reference threshold (red dashed line).

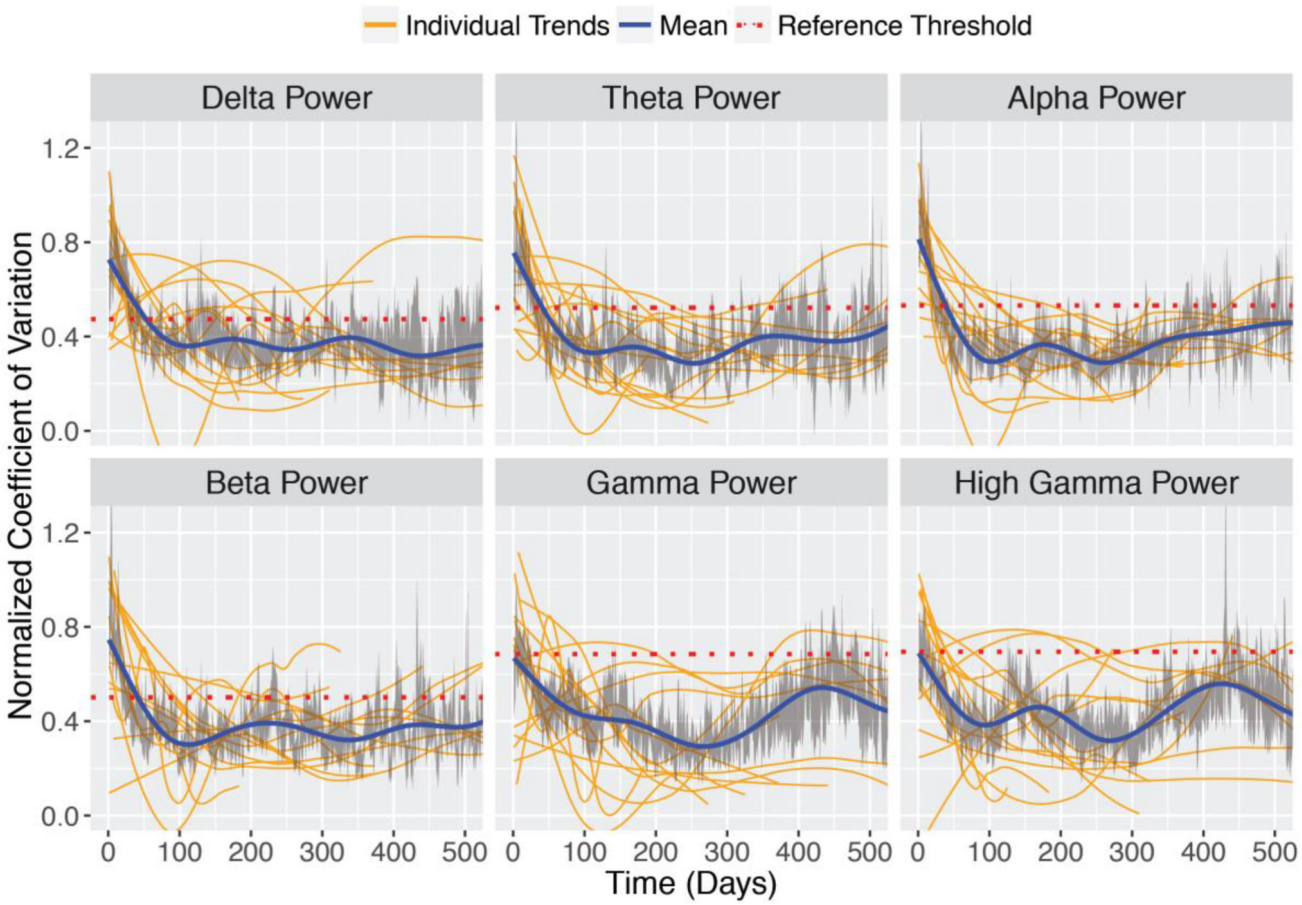

Figure 4. Coefficient of variation for spectral domain features

The mean coefficient of variation is shown for each feature with standard error bars in grey. Overlaid is the smoothed mean (blue) and reference threshold (red dashed line).

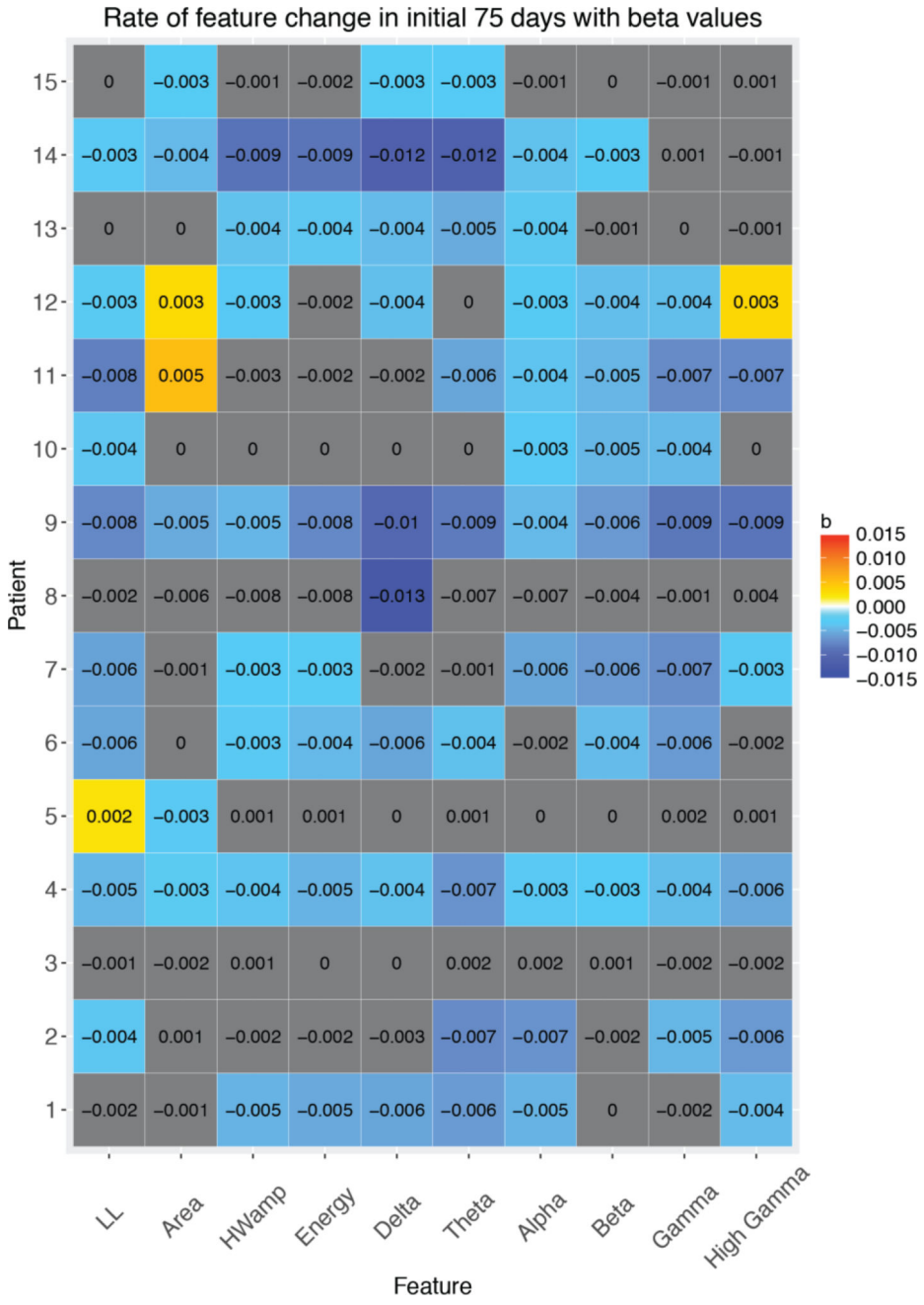

Figure 5. Individual variability

A linear model was fit separately for each patient for each feature from day 1 to day 75. Beta estimates (β_1, equation 2) for effect of time are shown here as well as on a color scale. The color scale indicates beta values (% change/day), with red indicating an increase in feature values and blue indicating a decrease. Grey indicates that the beta estimate for the patient/feature pair was not significantly different than 0 (no change) after False Discovery Rate (FDR) correction. LL = line length. Associated p values are given in Figure S7.

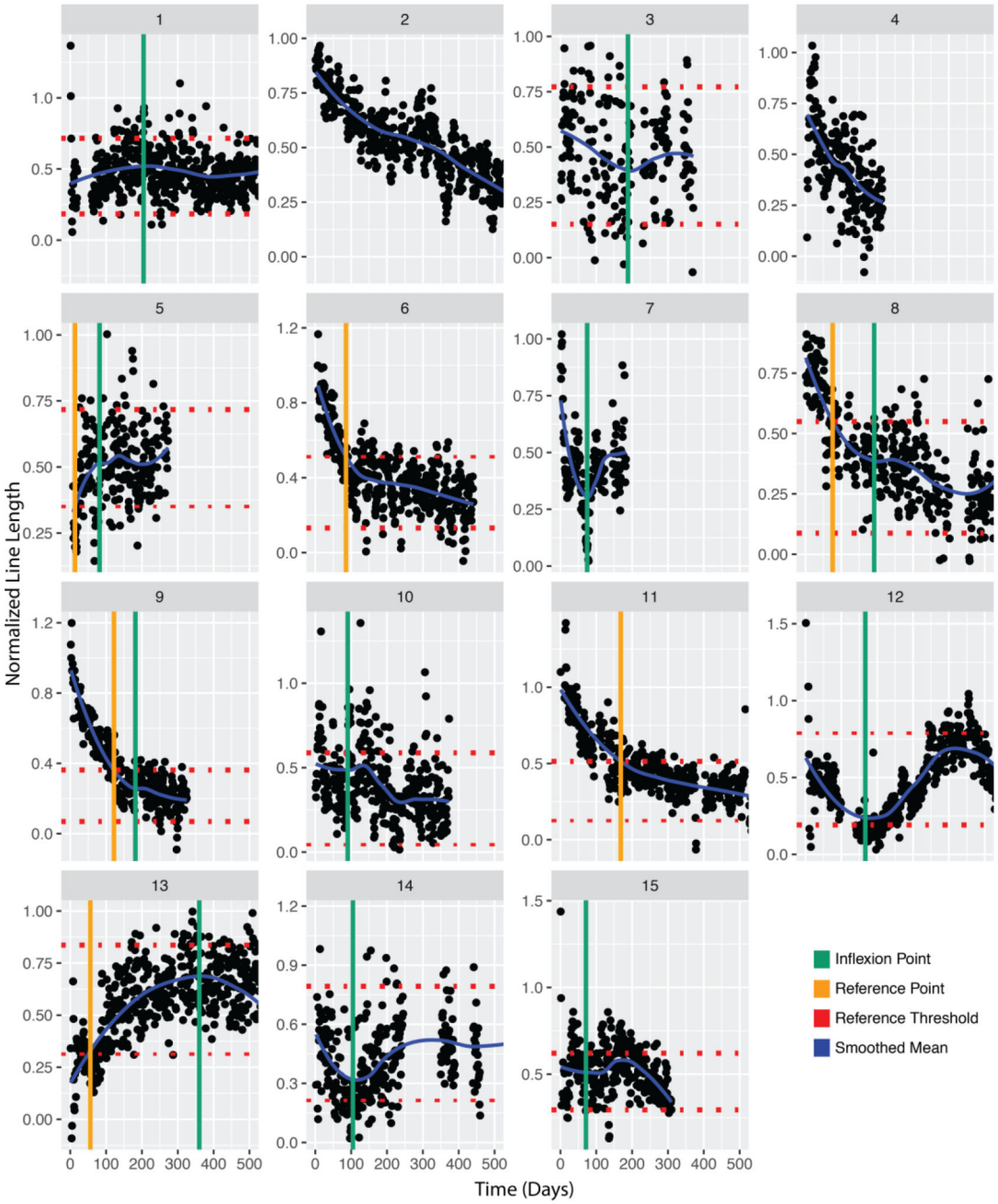

Figure 6. Normalized line length across days by subject

Each point represents the average value for a given day. Overlaid is the smoothed mean (blue) and reference threshold (red dashed line). The orange indicates the day feature values enter a reference range and the green line indicates the inflexion point.

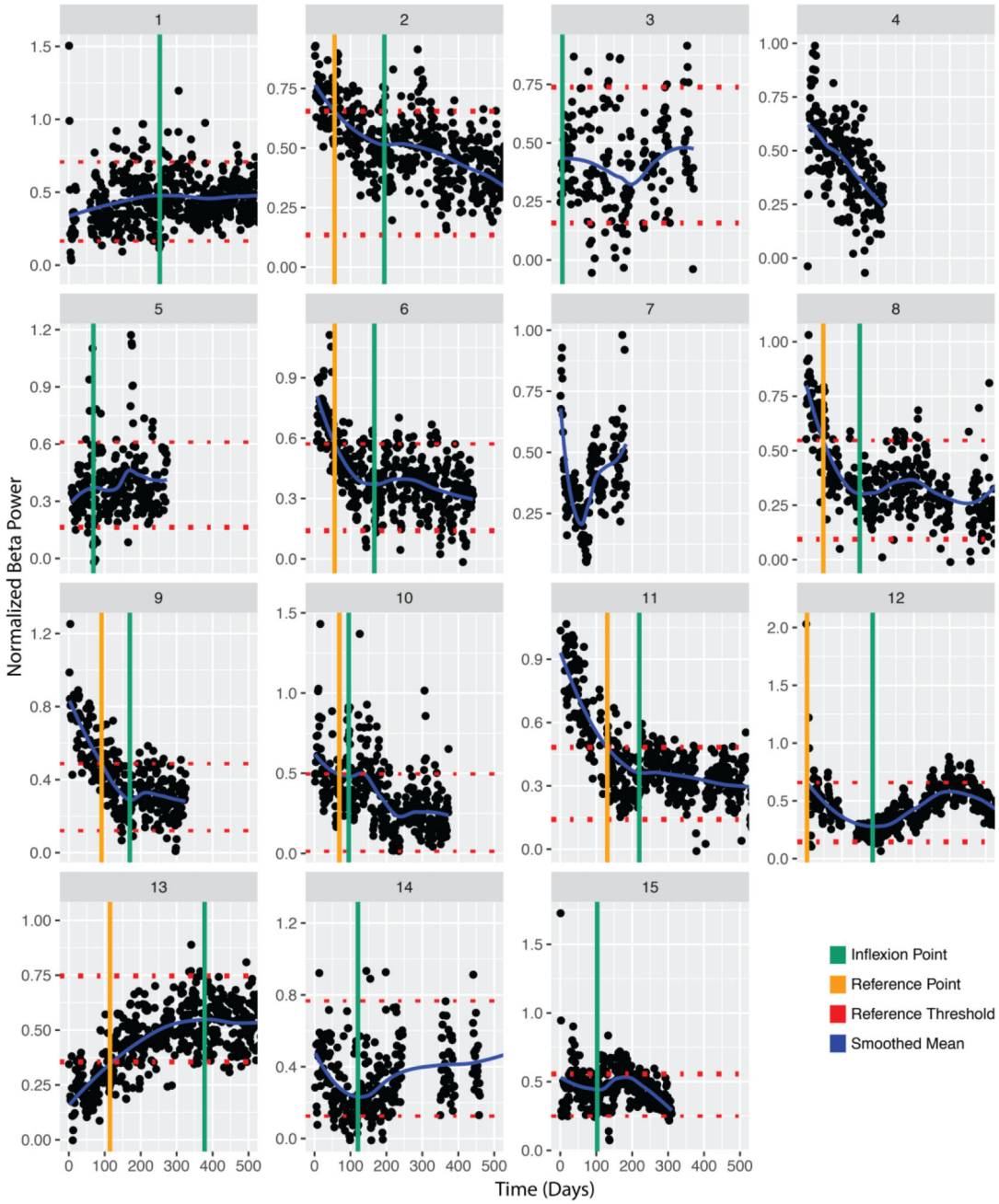

Figure 7. Normalized beta power across days by subject

Each point represents the average value for a given day. Overlaid is the smoothed mean (blue) and reference threshold (red dashed line). The orange indicates the day feature values enter a reference range and the green line indicates the inflexion point.

Table 1

Patient demographics and recording duration

Patient	Age	Sex	Diagnosis Age	Duration (Days)	Epileptogenic Zone
1	26	M	4	767.4	PT
2	44	M	12	730.1	OP
3	22	F	16	557.5	PT
4	61	M	48	233.0	PT
5	20	F	1	272.9	FT
6	62	M	37	441.3	T
7	52	M	26	184.9	FT
8	48	M	20	558.4	FT
9	51	F	10	394.9	OP
10	50	F	15	373.2	FT
11	53	F	15	721.6	FT
12	43	M	20	729.0	T
13	50	M	20	746.9	T
14	49	F	4	627.0	PT
15	36	M	5	465.6	T

PT = Parietal-Temporal, OP = Occipital-Parietal, FT – Frontal-Temporal, T = Temporal

Table 2

Days to reference range and inflexion.

	Days to reference range / inflexion	
Feature	**Temporal**	**Spatial**
Line Length	37.3 / 98	52.1 / 108
Area	* / 166	*
Half-wave	8.9 / 108	37.5 / 98
Energy	21.6 / 108	* / 311
Delta	17 / 108	52.5 / 98
Theta	23.5/ 108	41.6 / 98
Alpha	20.8 / 117	38.7 / 98
Beta	26.6 / 117	40.9 / 98
Gamma	42.9 / 98	* / 253
High Gamma	42.4 / 117	* / 88

For each feature, the time to the reference range is calculated as the first day when the mean value (or coefficient of variation) for each patient enters the defined reference range.

*within reference distribution at implantation. Corresponding values are given in Table 3.

Table 3

Normalized feature values at various points in time.

	Temporal Trend			Spatial Trend		
Feature	**Day 1**	**Reference**	**Inflexion**	**Day 1**	**Reference**	**Inflexion**
Line Length	0.641	0.538	0.442	0.985	0.555	0.335
Area	0.592	NA	0.411	0.469	NA	0.517
HW	0.584	0.564	0.400	0.796	0.558	0.338
Energy	0.561	0.506	0.366	0.522	NA	0.378
Delta	0.593	0.538	0.341	0.726	0.476	0.364
Theta	0.599	0.526	0.368	0.755	0.518	0.337
Alpha	0.571	0.521	0.383	0.813	0.531	0.294
Beta	0.579	0.516	0.386	0.746	0.505	0.307
Gamma	0.632	0.502	0.411	0.667	NA	0.296
High Gamma	0.580	0.501	0.437	0.689	NA	0.384

Normalized mean feature values on Day 1, on day when feature value enters the reference range, and at the inflexion point for both temporal and spatial variability. NA = indicates feature is always within the reference range.

Table 4

Linear mixed model estimates.

Feature	β_1(/Day)	SE	t(812)	Adj. P	β_0	% Change Day 1–75
Line Length	0.332	0.076	−4.346	<0.001	0.680	36.6
Area	0.118	0.075	−1.574	0.1160	0.605	14.7
HW	0.307	0.072	−4.280	<0.001	0.615	37.4
Energy	0.340	0.075	−4.542	<0.001	0.599	42.6
Delta	0.434	0.094	−4.636	<0.001	0.634	51.3
Theta	0.430	0.102	−4.200	<0.001	0.651	49.6
Alpha	0.318	0.060	−5.255	<0.001	0.610	39.1
Beta	0.295	0.063	−4.700	<0.001	0.615	35.9
Gamma	0.350	0.082	−4.276	<0.001	0.668	39.2
High Gamma	0.232	0.092	−2.522	0.0119	0.615	28.3

Linear mixed models were fit over all patients. The fixed effect of time is shown for each feature. P values are adjusted for FDR at 0.05. The estimated total percent change from Day 1 to Day 75 is calculated by as $\beta_0 - (\beta_1 * 75)$. SE = Standard Error, t(df) = t statistic, Adj. P = adjusted p value